Fluorescence correlation spectroscopy on electron transfer reactions : probing inter- and intramolecular redox processes

Sen, S.

Chapter 5

Labeling and fluorescence correlation spectroscopic studies on Lys122Ser and Lys122Gln mutants of Copper Azurin

Abstract

A detailed investigation of the products of the labeling reaction of K122S and K122Q Cu azurin variants with the oxazine fluorophore ATTO655 has been performed. Fluorescence correlation spectroscopy was performed to understand the behavior of the labeled products under redox conditions. In this work, we have tried to understand the ET reaction using a specific species where the label is likely to be attached on a surface lysine and it reports sub-millisecond ET reaction under redox conditions. Slower ET rates in variants of azurin than the rates in *wt* Cu azurin reveal that these lysine residues must be at least 20 Å away from the copper center. Two different mechanisms are equally likely to be involved in the ET event.

5.1 *Introduction*

Biological electron transfer (ET) is observed for many processes in living cells and organisms. These processes include respiration, photosynthesis, immune response, solar-energy conversion and collagen synthesis. In most of these processes, electron transfer reactions take place with the help of redox proteins, with a certain prosthetic group, a metal ion or an organic molecule, which mostly determines the redox properties of the protein(*1*)(*2*)(*3*). We have chosen the prototype electron transfer (ET) protein, copper azurin from *Pseudomonas aeruginosa* for investigating ET reactions(*4*). Azurin is easily obtained by heterologous expression in *E. coli* bacteria in high yields(*5*), and the protein is very stable at room temperature(*6*)(*7*)(*8*)(*9*). It also has a rigid scaffold for the metal-binding site, the properties of which are fine-tuned by the surrounding protein matrix. Thus, azurin is among the most extensively studied redox enzymes. It serves as a donor or acceptor for several other proteins and substances in bacteria(*10*)(*11*)(*12*). A remarkable amount of information is available in the literature regarding its spectroscopic, structural and ET properties(*13*)(*14*)(*15*). Also many variants have been studied.

Recent advances in optical imaging techniques have established that it is possible to observe the dynamics of a protein at single-molecule level(*16*)(*17*)(*18*)(*19*). Analytical measurements at the single-molecule level using fluorescence techniques have become almost routine in many research laboratories in the past few years. Among these techniques, single-molecule fluorescence correlation spectroscopy (FCS) has proven to be valuable to investigate a range of processes such as ligand binding, protein folding, protonation and deprotonation (*20*)(*21*)(*22*)(*23*)(*24*)(*25*)(*26*)(*27*)(*28*). Ultimate goal in these investigations is the direct investigation of the molecular dynamics *in vivo*. In previous chapters, the inter- and intramolecular electron transfer processes were addressed by a FRET (Fluorescence resonance energy transfer)-FCS based approach.

Labeling oxidoreductases with a fluorescent dye has allowed the study of enzyme turnover at single-molecule level, provided Förster resonant energy transfer (FRET) occurs between the label and the active site(*29*)(*30*)(*31*)(*32*)(*33*). Our previous investigations on ATTO655 (oxazine dye) labeled azurin have revealed that it is possible to purify protein labeled at a specific position from a mixture that is obtained after performing a labeling reaction of the protein with a dye(*34*). In the case of azurin, we addressed the fluorescent behavior of those individual components at the single-molecule level (see Chapter 3and 4 for details). That work

has enabled us to understand ET dynamics as a function of the position of the label on the protein surface. We have been able to monitor intramolecular ET dynamics in the microsecond region between the label attached at the K122 position of the protein surface and the metal center.

Interestingly, among all the lysine residues present in the protein (Lys 24, Lys27, Lys128, etc.) (Fig. 5.1), Lys122 was identified as the main reaction site during labeling with the NHS-ester of ATTO655(*34*). Subsequently, further questions arose relating to the microsecond ET process that emerged from the FCS curves of K122 labeled azurin. If single-molecule detection for ET dynamics is possible for K122 labeled Cu azurin, would it be possible to encounter the same decay in Cu azurin-ATTO655 bioconjugates where the reaction sites are other surface lysines of azurin (Lys24, Lys27, Lys128, etc.)? Will the time scale of intramolecular electron transfer in those cases be similar to our previous results?

In order to answer these questions, we have mutated the lysine residue at position 122 into a serine (K122S) and a glutamine (K122Q). In the present study, our strategy was to label the variants with ATTO655, to characterize the products of the labeling reaction and then study the properties of a specific species by means of FCS. Singly labeled azurin derivatives were separated from one another and purified by ion exchange chromatography. The redox properties of the solution containing the azurin-dye constructs were manipulated by using potassium hexacyanoferrate (III) and sodium ascorbate. The reaction rates of the photoinduced electron transfer from the Cu(I) ion to the label and for the back reaction from the label to the Cu(II) were obtained from FCS measurements. Analysis of the obtained rate constants for electron-transfer to or from the copper center revealed a good correlation between the time scale of ET and the length of the ET pathway.

5.2 *Materials and Methods*

5.2.1 *Chemicals*

Unless stated otherwise, all materials were purchased from Sigma-Aldrich Corp. St. Louis, USA and used as received.

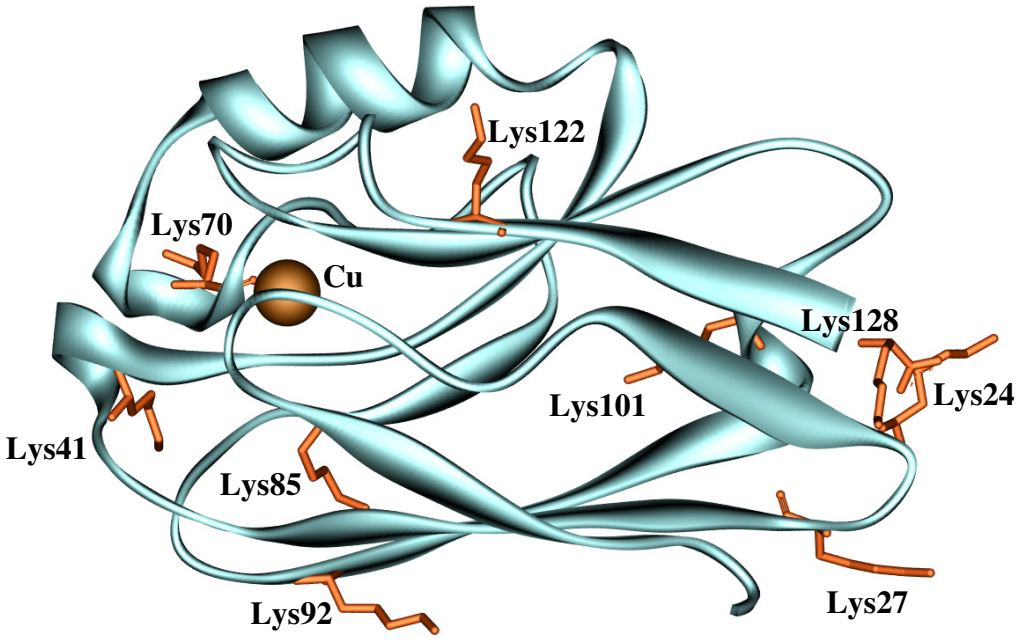

Figure 5.1: *Cartoon representation of the structure of azurin with its surface lysine residues (PDB: 2AZU). The copper ion is displayed as a brown sphere. The lysine amino acids are represented by red sticks. The model of azurin was prepared by using the DS visualizer program (Accelrys Discovery Studio 2.0).*

5.2.2 *Site-directed mutagenesis and proteins*

Lys122 to Ser (K122S) and Lys122 to Gln (K122Q) mutations were introduced into the azurin gene by site-directed mutagenesis (QuikChange Site-directed mutagenesis kit-Stratagene). The primers used for the respective mutations are given below; mutations are in bold and underlined. Primers were designed using the provided software of the QuikChange kit.

K122S_forward	5'-gtcagggtgcc**gc**tcatcagtgcgctatgacccg-3'
K122S_reverse	5'-cgggtcatagcgcactgatga**gc**ggcaccctgac-3'
K122Q_forward	5'-catagcgcactgatg**c**aaggcaccctgaccc-3'
K122Q_reverse	5'-gggtcagggtgccttg**c**atcagtgcgctatg-3'

Desired mutations were confirmed by DNA sequencing (BaseClear). The codon optimized gene was synthesized by Life Technologies and was cloned into pET28 vector. The expression and the

purification of the mutants were carried out as reported previously(*5*). The proteins were aliquoted and stored at -80 ºC till further use. Models for the variants are displayed in Fig. 5.2. The absorption spectrum of *wt*-Cu Azurin, K122S, and K122Q variants are shown in Fig. 5.3.

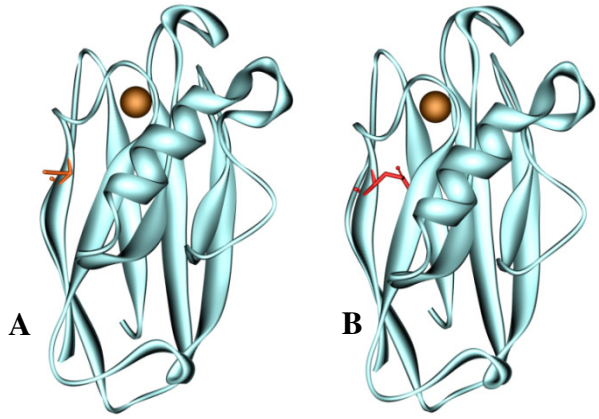

Figure 5.2: *Models for K122S (A) and K122Q (B) variants. The Models were generated by using "WhatIf molecular modelling program", Radboud University, The Netherlands (G. Vriend, J. Mol. Graph., 1990, 8, 52-26). Visual rendering of the molecules was performed by using the DS visualizer program (Accelrys Discovery Studio 2.0). The copper ion is displayed as a brown sphere. Serine122 and Glutamine122 residues are presented as red sticks.*

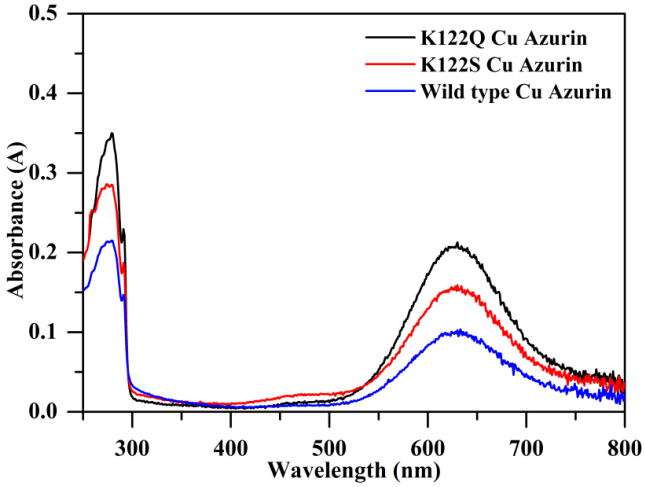

Figure 5.3: *Absorption spectra of wt (20 µM), K122S (30 µM) and K122Q (35 µM) Cu Azurin. The spectra were measured in 20 mM HEPES, pH 7.0 at room temperature.*

5.2.3 *Protein labeling and chromatography of labeled species*

K122S and K122Q Cu-azurin from *Pseudomonas aeruginosa* were labeled using commercially available N-hydroxysuccinimidyl-ester (NHS) of ATTO655 dye (ATTO-TECH, GmbH, Germany). Elimination of the unreacted label from the labeling mixture and separation of the different labeled species using ion exchange chromatography were executed as previously reported(*34*). Labeling at pH 6.0 and pH 7.0 was performed using 20 mM HEPES. UV/Vis spectra were measured on a Cary50 UV/Vis (Varian Inc. Agilent Technologies, USA) spectrophotometer.

5.2.4 *Fluorescence switching in bulk*

Fluorescence spectroscopy experiments were carried out using a Cary Eclipse Spectrophotometer (Varian Inc. Agilent Technologies, USA). The experiments were performed in 20 mM HEPES, pH 7.0 at room temperature and the concentration of the labeled samples was 50-100 nM. The experiments were performed as previously described (See Chapter 3). Details on the measurement of the fluorescence switching ratio have been discussed in Chapter 1.

5.2.5 *Sample preparation for FCS experiments*

Samples were prepared as discussed in Chapter 2 and 3. They contained 57.0% sucrose (w/w) (viscosity 37.5 cP at 22^0C)(*35*). All solutions were passed through a 0.22 μm filter to avoid the presence of particulate. The final sample concentration of labeled protein was around 0.4-0.8 nM. Manipulation of the redox potential of the solution was established by employing potassium hexacyanoferrate (III) and sodium ascorbate as oxidizing and reducing agents, respectively.

5.2.6 *Fluorescence Correlation Spectroscopy setup and data acquisition*

FCS experiments were performed on a home-built confocal setup equipped for Time-Correlated Single-Photon Counting (TCSPC) measurements (See Chapter 2 for details). All experiments were performed at ambient temperature (22 ºC). Excitation at 639 nm was provided by a pulsed diode laser head (LDH-P-C-635-B, 20 MHz rep rate, PicoQuant GmbH, Berlin, Germany) driven by a picosecond laser driver (LDH-800-B, PicoQuant GmbH, Berlin, Germany). The power used for the calibration and for the FCS measurements amounted to 20

μW, as measured after the objective, corresponding to a specific power of ~4.3 kW/cm^2 at the sample.

For the acquisition of the FCS data, 80 μl of the sample solution was deposited onto a glass slide (cover slips Nr. 1.5, thickness 0.16 - 0.19 mm, Gerhard Menzel GmbH, Germany) and covered with the cap of a polypropylene test tube to prevent evaporation of the solvent during the measurements. The focus was set at a distance of 20 μm from the upper surface of the glass coverslip to prevent detection of fluorescence from surface-adsorbed molecules. Time traces were recorded with the SymPhoTime software package (PicoQuant GmbH, Berlin, Germany) for durations varying from 5 to 10 minutes. Raw data were stored as time-tagged time-resolved (t3r) data files and subsequently elaborated by using the SymPhoTime software package.

5.2.7 *FCS data analysis*

After acquisition of the data, the time-correlated single photon counting (TCSPC) histogram was built, and fitting was performed after narrowing down the time window of the TCSPC decay. The autocorrelation functions were analyzed by fitting to the following equation(*26*):

$$G(\tau) = G(0) \cdot G_{diff}(\tau) \cdot G_1(\tau) \cdot G_2(\tau) \qquad (5.1)$$

where $G(0)$ is given by

$$G(0) = \frac{1}{\langle N \rangle} = \frac{1}{c \cdot V_{eff} \cdot N_A} \qquad (5.2)$$

$G_2(\tau)$, or both $G_1(\tau)$ ànd $G_2(\tau)$, were omitted when their inclusion in the fitting procedure gave no significant improvement of the fit. Fitting of the autocorrelation data was performed in GraphPad Prism 5 or 6.05 (GraphPad Inc., USA). The quality of the fits was judged by visual inspection of the residuals.

5.3 *Results and discussion*

5.3.1 *Purification of labeled species and characterization*

To isolate a homogeneous 100% singly labeled sample from the labeling solution, ion exchange chromatography (IEC) of the reaction mixture was performed following the protocol mentioned in(*34*). Fig. 5.4 shows the chromatogram of the labeling mixture of K122Q CuAzurin after reaction with ATTO655 dye. Each peak corresponds to a different species. The fractions were eluted under a gradient of 0 to 100 mM sodium chloride in 5 mM Tris pH 8.5 over 30 column volumes at a flow rate of 0.5 ml/min. The concentrations of the fractions were determined from the extinction coefficients $\mathcal{E}_{\text{Azurin}}^{280}$ = 9.8 $\text{mM}^{-1}\text{cm}^{-1}$ and $\mathcal{E}_{\text{dye}}^{663}$ = 125 $\text{mM}^{-1}\text{cm}^{-1}$ by UV/Vis spectrometry(*36*). K122S Cu azurin-ATTO655 displayed an elution profile similar to K122Q. The UV/Vis spectra of the various species are grouped in two panels in Fig. 5.5. In panel A the spectrum corresponding to fraction 1 is that of unlabeled reduced K122S Cu azurin. Fraction 1' (P1') and fraction 2 (P2) show a main peak around 663 nm and a shoulder at 618 nm. This pattern matches the spectrum of singly labeled azurin(*37*). Fractions 3 (P3) and 4 (P4) show a major peak at 615 nm and a less intense peak at 663 nm, reminiscent of H-type dimerization of ATTO dyes(*38*). Fractions 3-5 for both variants were not investigated further.

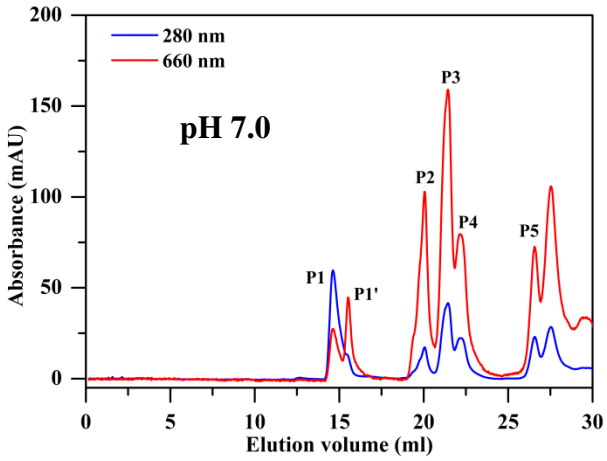

Figure 5.4: *Elution profile of the reaction mixture after performing the labeling reaction for K122Q with the NHS ester of ATTO655 at 20 mM HEPES, pH 7.0. The elution was performed in 5 mM Tris buffer, pH 8.5 with a 0 to 100 mM NaCl gradient over 30 column volumes at a flow rate of 0.5 ml/min. Numerical tags are used to identify peaks. The chromatograms show the elution pattern when monitoring at two wavelengths: 280 nm (blue line), characteristic absorption of the protein; and 660 nm (red line), characteristic absorption of the label.*

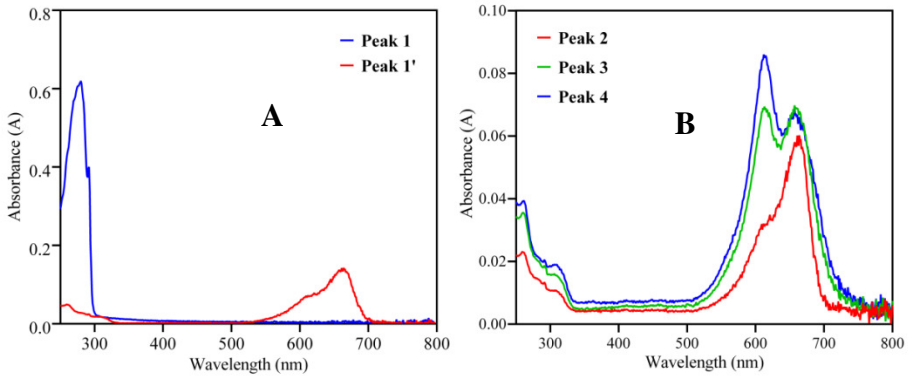

Figure 5.5: *UV/Vis spectra of the fractions isolated during chromatographic separation from K122S Cu azurin-ATTO655 labeling mixture. The species are identified by the tag numbers used in Fig. 5.4.*

5.3.2 *Influence of the pH on the labeling reaction*

To investigate the product distribution for these variants, we performed the labeling reactions at different pH values (6.0 and 7.0). In case of the K122S mutant (Fig. 5.6), when comparing the intensities of the first four fractions with one another, it is clear that when going from pH 6.0 to pH 7.0, fraction 1' and fraction 2 decrease and fraction 3 increases. As a general effect, an increase in pH increases slightly the yield of the labeling reaction. For both mutants, when comparing the relative intensities, the amount of fraction 1' was found to be lower than that of fraction 2 at pH 7.0. In the present case, fraction 1 is assigned to unlabeled reduced azurin as it shows no absorbance at 660 nm.

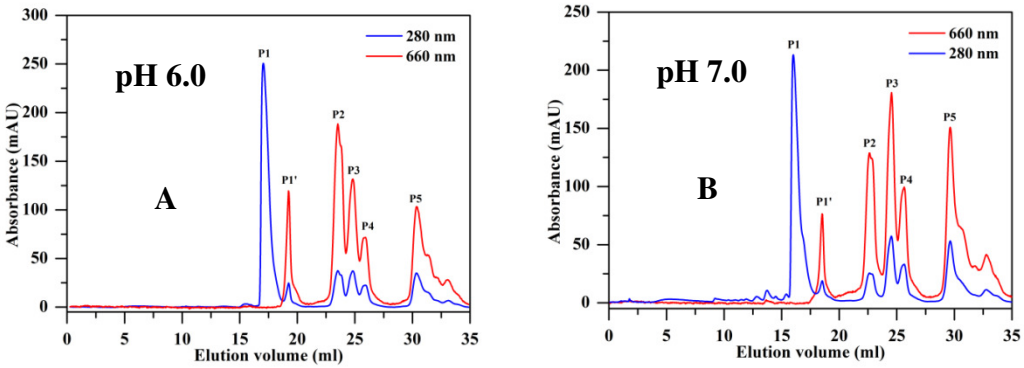

Figure 5.6: *Elution profiles of the reaction mixtures for the K122S variant after performing the labeling reaction at different pHs as indicated in the top left corner of each panel. The conditions used for the separation are the same as indicated for Fig. 4. Numerical tags are used to identify peaks.*

The pK_a values of lysine122 and the N-terminus are known (~ 7.0 and 8.0 respectively). But pK_as of other surface lysines (Lys24, Lys27, Lys41, Lys128, etc.) are not available in the literature. It is expected that these lysine residues have pK_as higher than the pK_a of K122(*39*). Increasing pH to 7.0 or higher makes those lysines available for labeling with dye. We choose fraction 1' and fraction 2 for further investigation.

5.3.3 *Fluorescence switching experiments*

For each species, the sample was excited at 660 nm, and the fluorescence emission was monitored at 685 nm after addition of redox agents (See Fig. 5.7). Upon addition of oxidant, the fluorescence drops, the magnitude of the drop depending on the initial redox state of the protein. Subsequent addition of reductant produces an increase of the fluorescence. This cycle was repeated, and the switching ratio was calculated for each fractions. Details about the calculation of the switching ratio have been discussed in Chapter 1. Table 5.1 presents the measured switching ratios.

N-hydroxysuccinimide (NHS) ester-mediated derivatization generally involves the reaction of the amine-reactive group with the primary amines of a protein or a biomolecule. We may expect that ATTO655 is not reactive towards a serine or glutamine residue at the 122 position of the protein. From experimentally obtained FRET efficiency or switching ratios and comparing the results with our previous work(*34*), it is tentatively proposed that the position of the label in fraction 1' is the N-terminus and that fraction 2 must contain a species where the label is attached to a lysine moiety close to the copper center. In the present work, further investigation was performed only on fraction 2.

Fractions	**Switching ratio**
fraction 1'	0.68
fraction 2	0.83

Table 5.1: *Experimentally obtained switching ratios for fraction 1' and fraction 2.*

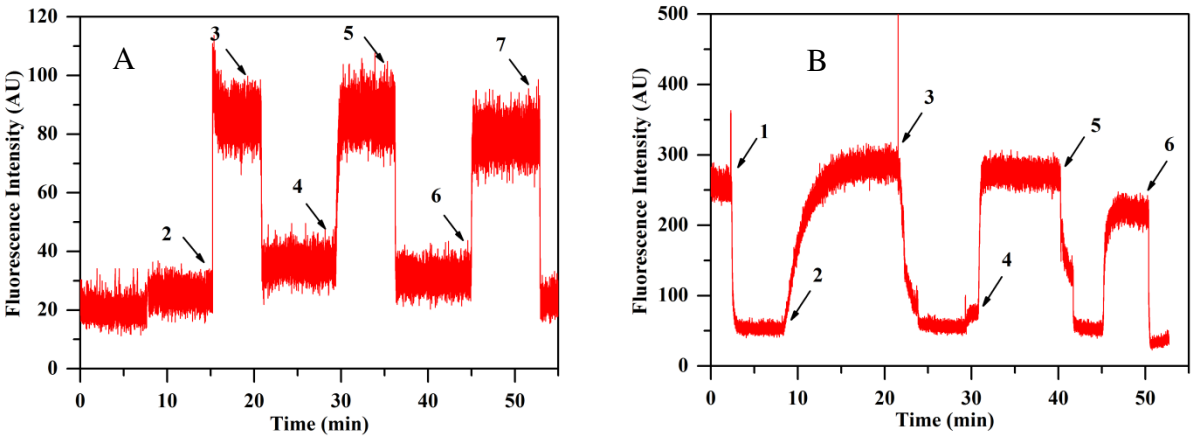

Figure 5.7: *Fluorescence switching experiments on 50 nM of ATTO655 labeled K122S copper azurin in 20 mM HEPES, pH 7.0 at room temperature. The black numbers mark the addition of oxidant and reductant in the samples. A: fraction 1', B: fraction 2. The time points 1, 3, 5, and 7 correspond to the addition of 0.05, 1, 6, and 18 mM (final concentrations) of potassium ferricyanide to the sample, respectively. The time points 2, 4, and 6 correspond to the addition of 0.25, 1.5, and 4.5 mM of sodium ascorbate (final concentrations), respectively.*

5.3.4 *FCS experiments*

FCS experiments were performed in 57% (w/w) sucrose solutions at room temperature (295 K) in 20 mM HEPES buffer pH 7.0. Redox conditions were controlled by the addition of potassium hexacyanoferrate (III) as oxidant and sodium ascorbate as reductant.

5.3.4.1 *K122Q CuAzurin-ATTO655, fraction 2, under oxidizing conditions*

When titrating K122Q -CuAzu with hexacyanoferrate(III), the observed ACFs could not be fit adequately with the equation containing a single diffusion term (Fig. 5.8) and a two-term function with $G_{diff}(\tau)$ and $G_1(\tau)$ was used to fit the data (Fig. 5.9). Fitting with two terms still did not produce optimal fits (Fig. 5.9), but including a third term $G_2(\tau)$ in the FCS equation did not markedly improve the plot of the residuals.

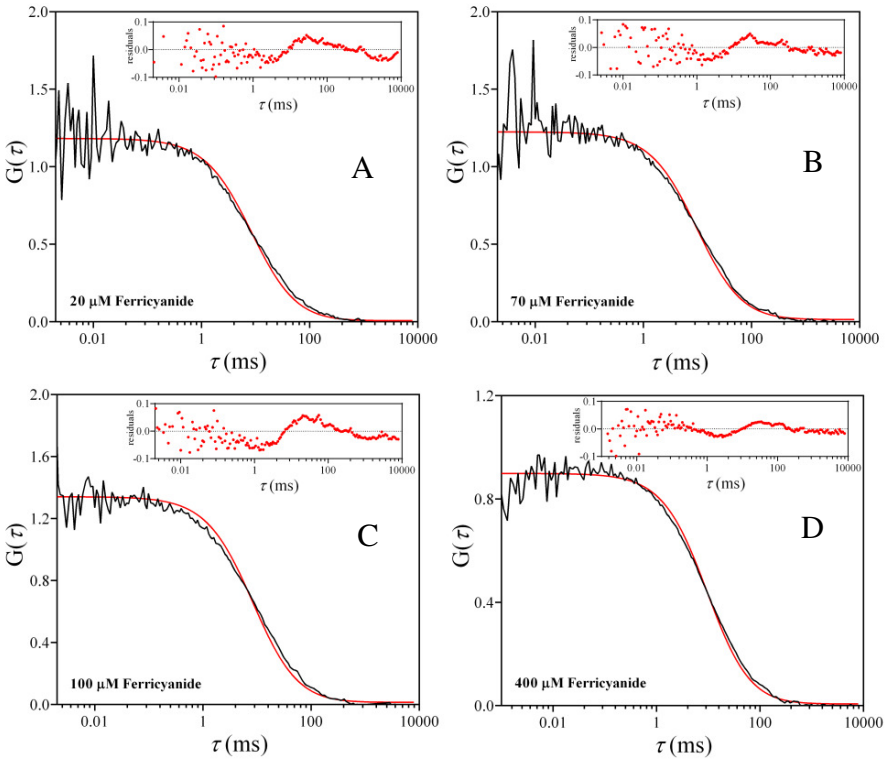

Figure 5.8: *Experimentally obtained ACFs of fraction 2 from K122Q Cu azurin labeled with ATTO655 for samples containing 10 (A), 40 (B), 300 (C) and 500 (D) µM hexacyanoferrate (III). The red lines are fits according to Eqn. 3.1 G(τ) = G(0).G_{diff}(τ). The residuals of the fits in the insets show unsatisfactory fitting of the ACFs.*

Thus, it is clear that next to the diffusion term a blinking term is needed to fit the experimental ACF. After analysis, both F_1 and τ_1 (F_1 is the fraction of molecules associated with the blinking reactions, and τ_1 is the relaxation time required for that reaction, see Chapter 4 for details) appeared independent of the ferricyanide concentration with F_1 = 0.16 and τ_1 = 0.68 ms (Fig. 5.10). This blinking reaction was not observed in the case of the Zn containing *wt* azurin (See Chapter 3) and so the Cu center must be involved in this reaction (Scheme 5.1)

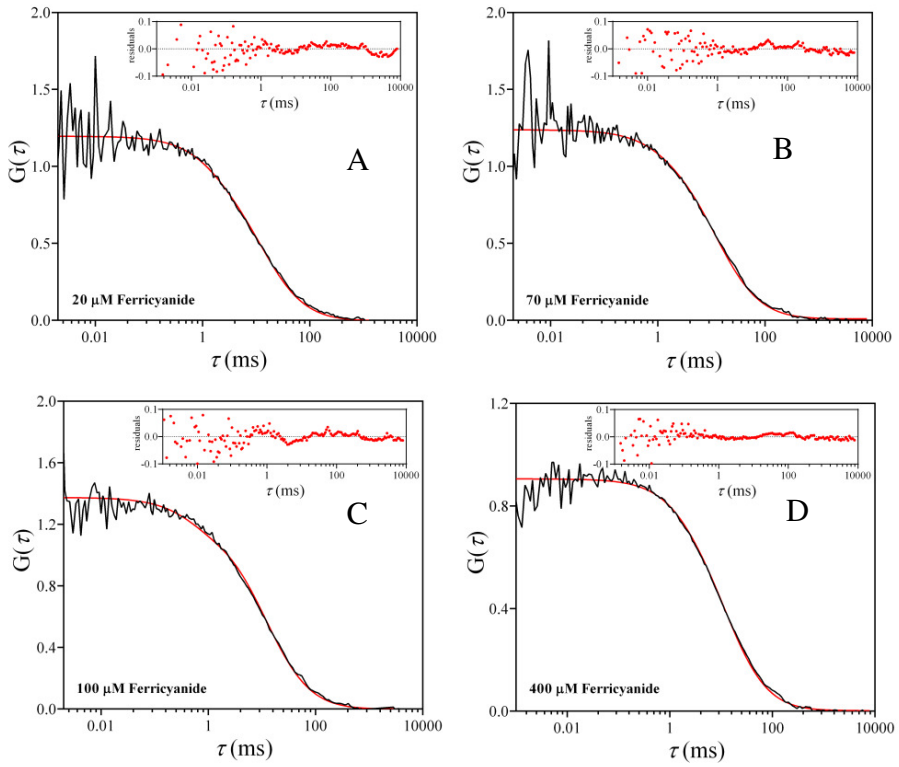

Figure 5.9: *Experimentally obtained ACFs of fraction 2 from K122Q Cu azurin labeled with ATTO655 for samples containing 20 (A), 70 (B), 100 (C) and 400 (D) µM hexacyanoferrate (III). The red lines are fits according to Eqn. 3.4* $G(\tau) = G(0).G_{diff}(\tau).G_1(\tau)$ *with* $\tau_D = 12$ *ms.*

$$LCu(II) \underset{k_{10}}{\overset{k_{01}}{\rightleftharpoons}} L^*Cu(II) \xrightarrow{k_1^f} L^+Cu(I) \xrightarrow{k_1^b} LCu(II)$$

.

Scheme 5.1: *Light induced ET reactions in oxidized CuAz. LCu symbolizes the labeled azurin molecule in which the Cu is in the reduced or oxidized form (Cu(I) or Cu(II), respectively) and the label, L, is excited or oxidized (L* or* L^+*, respectively). The rates for intramolecular ET from L* to Cu(II) and from Cu(I) to* L^+ *are denoted by* k_1^f *and* k_1^b.

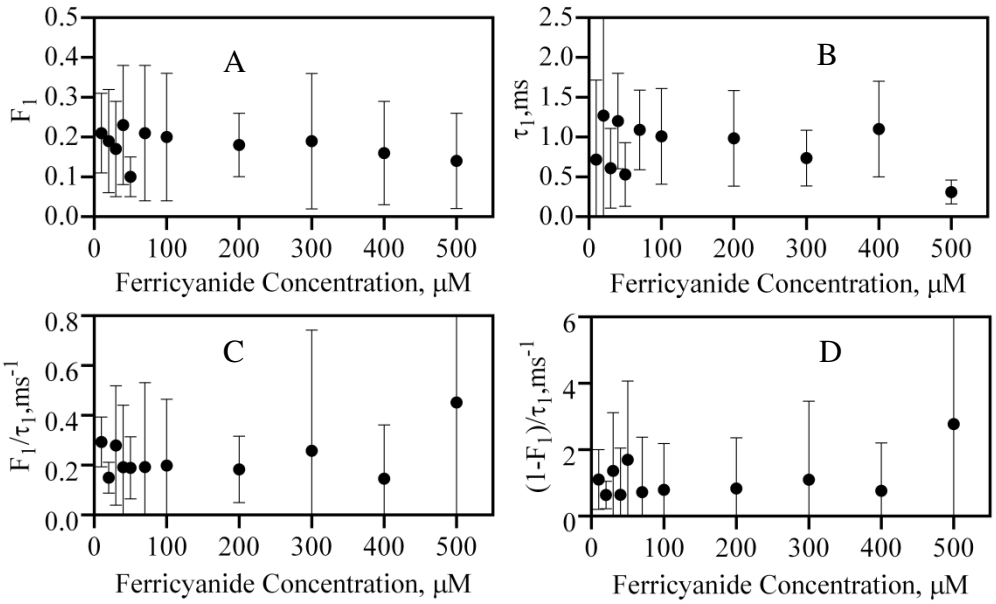

Figure 5.10: *(A) and (B): Parameters (F_1 and τ_1) obtained by fitting the ACFs of K122Q labeled Cu azurin as a function of the concentration of added hexacyanoferrate (III). The equation used for the fits was $G(\tau) = G(0).G_{diff}(\tau).G_1(\tau)$ with τ_D =12 ms. (C) and (D):$(1-F_1)/\tau_1 = k^b$ and $F_1/\tau_1 = k^f$ are plotted as a function of potassium hexacyanoferrate (III) concentration, respectively. Vertical bars denote 95% confidence intervals.*

Consistent with the intramolecular character of the reaction, neither F_1 nor τ_1 appears to depend on the concentration of oxidant (Fig. 5.10 A-B). Following the formalism discussed in Chapter 4, one obtains

$F_1/\tau_1 = f(I)\ k_1^f$ and

$(1-F_1)/\tau_1 = k_1^b$.

k_1^f and k_1^b are the forward and backward ET rate constants under Scheme 5.1. In oxidized azurin the label fluorescence is partly quenched by the Cu center and the fluorescence life time is shortened to 1.8 ns (See Chapter 4 for details and Fig. 4.5). It leads to $f(I) = 3.2\times10^{-3}$ where the factor $f(I)$ can be understood by considering that the optically excited label reacts with oxidant in the solution (see Chapter 4 for details). With F_1 = 0.16 and τ_1= 0.54 ms, one obtains k_1^f =

6.1×10^4 s^{-1} and k_1^b = 1.2×10^3 s^{-1}. As before (see Chapter 4), these values can be used to obtain the reorganization energy for electron transfer.

With $E_{ATTO+/ATTO}$ = 1.55 V (vs NHE) and $\Delta G_{0,0}$ = 1.86 eV(*40*), n_{ATTO} = 0, $n_{Cu(II)}$=2 and a midpoint potential of azurin at pH 7 of 0.31 V (vs NHE)(*41*)(*42*), one obtains driving forces of ΔG_f = -0.476 eV and ΔG_b = -1.384 eV for the reactions shown in Scheme 5.1. This, finally leads (see details in Chapter 4) to λ (K122Q) = 0.76 eV.

5.3.4.2 K122Q Cu Azurin-ATTO655, fraction 2, under reducing conditions

Fluorescence time traces were recorded of 0.5-1 nM solutions of fraction 2 of K122Q Cu Azu-ATTO655 in 57% w/w (i.e. 70% w/v) sucrose in the presence of varying amounts (0-500 μM) of ascorbate. For each time trace the autocorrelation function was calculated. It appears that application of $G(\tau) = G(0)\, G_{diff}(\tau)$ and/or $G(\tau) = G(0)\, G_{diff}(\tau)\, G_1(\tau)$ did not result in good fits: and the residuals exhibited a noticeable non-random component (Fig. 5.11). Then the ACFs were fit with an equation containing an additional term $G_2(\tau)$ ($G(\tau) = G(0)\, G_{diff}(\tau)\, G_1(\tau)\, G_2(\tau)$) (see Eqn. 5.1) with the diffusion correlation time fixed at τ_D = 12 ms (Fig. 5.12). Including the third term $G_2(\tau)$ in the Eqn. 5.1 resulted in good fits.

The amplitudes F_1 and F_2, and the corresponding correlation times, τ_1 and τ_2 are presented in Fig. 5.13. After fitting the ACFs, it was clear that K122Q-labeled CuAz-fraction 2 is involved in a reaction that occurs on a time scale of 400-500 μs. Similar to our previous experiments on *wt* Cu azurin, this reaction is ascribed to intramolecular ET from the Cu(I) site to the excited label and back (Scheme 5.2). In case of K122Q variant, with F_2 = 0.23, τ_2 = 0.23 ms and $f(1)$= 4.8×10^{-3} under reducing conditions (lifetime of the dye is 2.7 ns under reducing conditions, See Chapter 4, Fig. 4.5), one finds k_2^f = 2.1×10^5 s^{-1} and k_2^b = 3.3×10^3 s^{-1}. Using these rates and $E_{ATTO/ATTO-}$ = -0.17 V (vs ~ NHE), n_{ATTO} = 0 and $n_{Cu(I)}$=1 (See Chapter 4), one obtains λ (K122Q) = 1.08 eV.

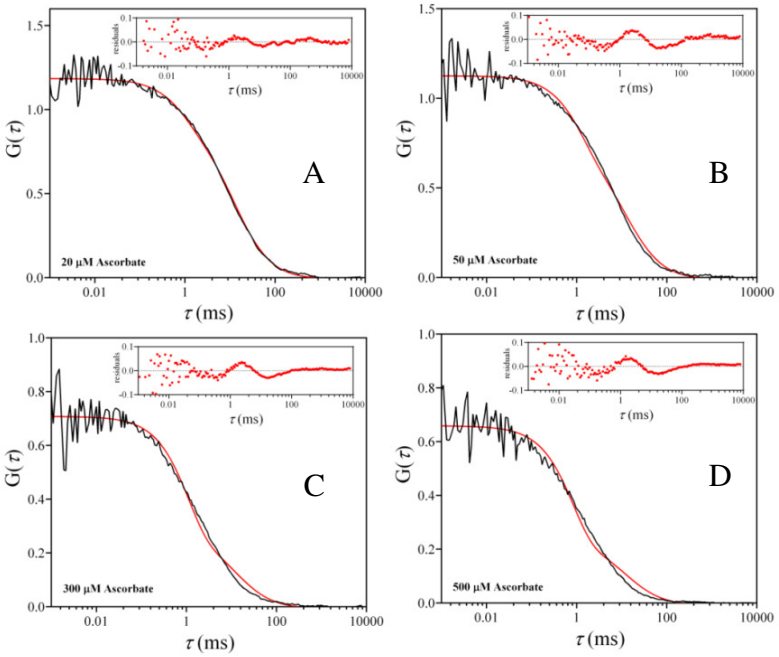

Figure 5.11: *Experimentally obtained ACFs of K122Q Cu azurin labeled with ATTO655, fraction 2, for samples containing 20 (A), 50 (B), 300 (C) and 500 (D) µM ascorbate. The red lines are fits according to* $G(\tau) = G(0).G_{diff}(\tau).G_1(\tau)$ *with* $\tau_D = 12$ *ms. The residuals in the insets show unsatisfactory fitting of the ACFs.*

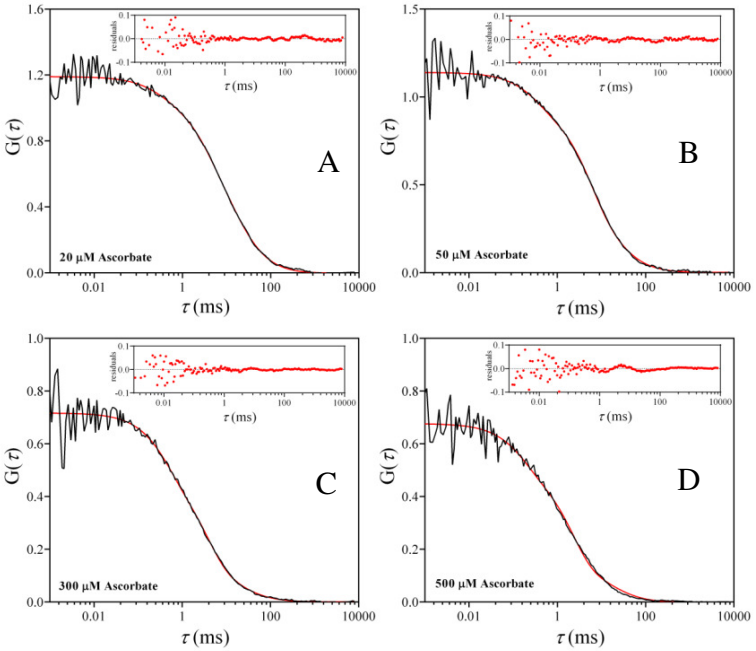

Figure 5.12: *Experimentally obtained ACFs of K122Q Cu azurin labeled with ATTO655, fraction 2, for samples containing 20 (A), 50 (B), 300 (C) and 500 (D) µM ascorbate. The red lines are fits according to Eqn. 5.1* $G(\tau) = G(0).G_{diff}(\tau).G_1(\tau)\ G_2(\tau)$ *with* $\tau_D = 12$ *ms. The residuals in the insets show satisfactory fitting of the ACFs.*

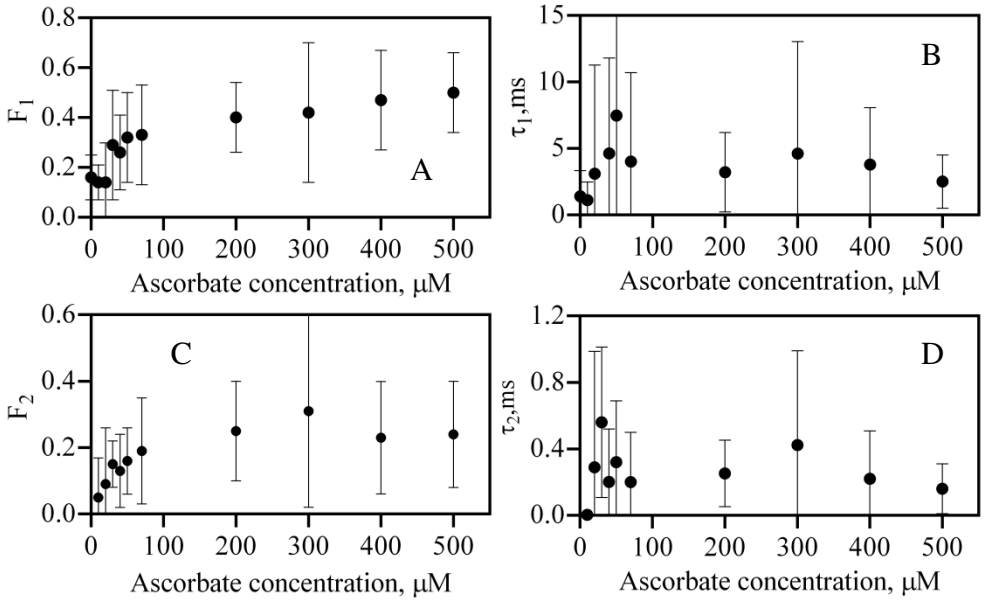

Figure 5.13: *Parameters obtained from the fits of the ACFs of fraction 2 (K122Q Cu azurin-ATTO655). The equation used was* $G(\tau) = G_{diff}(\tau)\, G_1(\tau)\, G_2(\tau)$ *with* $\tau_D = 12$ *ms. Shown are, as a function of ascorbate concentration:* F_1 *(A),* τ_1 *(B),* F_2 *(C), and* τ_2 *(D).*

$$LCu(I) \underset{k_{10}}{\overset{k_{01}}{\rightleftharpoons}} L^{*}Cu(I) \xrightarrow{k_2^{f}} L^{-}Cu(II) \xrightarrow{k_2^{b}} LCu(I)$$

Scheme 5.2: *Light induced ET reactions in reduced CuAz. Symbols have the same meaning as in Scheme 2. The rates for intramolecular ET from Cu(I) to L* and from L⁻ to Cu(II) to are denoted by* k_2^f *and* k_2^b.

$G_1(\tau)$ is related to the reduction of the label by the reductant and F_1 and τ_1 are analysed as before (See Chapter 4 for details), taking into account that only a fraction (1-F_2) of the labeled molecules is in the bright state. From the experimentally determined value of $k_r f(I)$ a value of k_r can be extracted after an estimate of $f(I)$ has been obtained (k_r is the second order rate constant for the reduction of the dye, See Chapter 3 for details). Fluorescence lifetimes of the labeled variants were found to be similar to labeled *wt* copper azurin (1.8 ns and 2.7 ns under oxidizing and reducing conditions respectively). With a fluorescence lifetime of 2.7 ns (See Chapter 4), an incident light intensity of 4.3 kW/cm^2 at 636 nm and an absorbance cross-section of the label of 1.3×10^{-16} cm^2 (based on an estimated $\varepsilon_{636} = 8\times10^4$ M^{-1}cm^{-1}), one finds that $\sigma I_{exc} = 1.80\times10^6$ s^{-1}

and $f(I)$=4.8×10^{-3}. Taking K122Q Cu azurin under reducing condition as an example, with k_r $f(I)$=3.4×10^5 M^{-1}s^{-1}, a value of k_r = 7×10^7 M^{-1}s^{-1} is obtained. As discussed in Chapter 2, considering that the experiments were performed in 70% (w/v) sucrose solutions, this is of the order of a diffusion-controlled reaction rate. The analysis is presented in the Fig. 5.14 and data are gathered in Table 5.2.

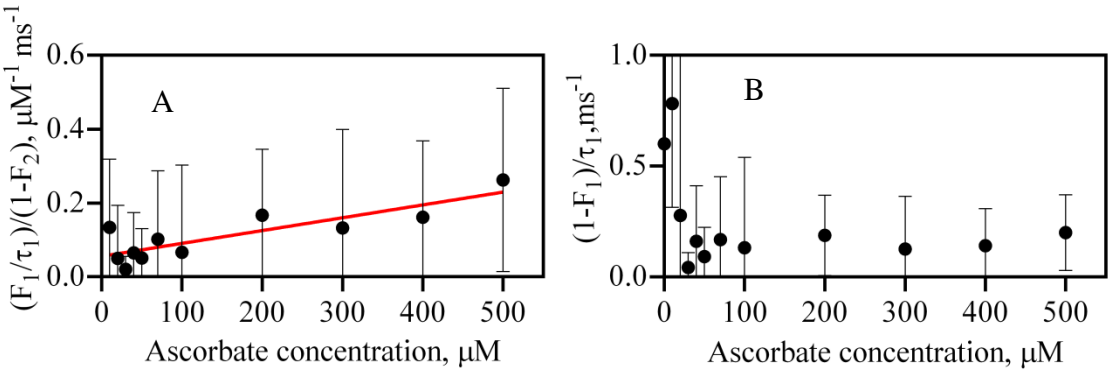

Figure 5.14: *Analysis of the ACFs of labeled Cu azurin variant (K122Q-fraction 2). ACFs were fitted with the equation $G(\tau) = G(0)\ G_{diff}(\tau)\ G_1(\tau)\ G_2(\tau)$ with τ_D =12 ms. Parameters τ_1 and F_1, as obtained from the fits, correspond with $G_1(\tau)$. (A) $(F_1/\tau_1)/(1-F_2)$ $(=k_f)$ as a function of the concentration of ascorbate for K122Q (B) and (B) $(1-F_1)/\tau_1$ $(=k_b)$ as a function of the concentration of ascorbate for the same variant. The red straight line is least-squares fit to the data points.*

k_b appears to be constant, which is consistent with the idea that dissolved oxygen is responsible for the back oxidation of the label as oxygen is present in the solution in large excess and its concentration will not change appreciably over the duration of the experiment. This has been discussed in Chapter 3. Data for the variants are gathered in Table 5.2.

5.3.4.3 K122S Cu Azurin-ATTO655, fraction 2, under oxidizing conditions

When titrating K122S -CuAzu with hexacyanoferrate(III), the observation was similar to K122Q. A two-term function with $G_{diff}(\tau)$ and $G_1(\tau)$ was needed to fit the data properly (Fig. 5.15). Fitting with two terms still did not produce optimal fits, but including a third term $G_2(\tau)$ in the FCS equation did not markedly improve the plot of the residuals. The data is gathered in Fig. 5.16.

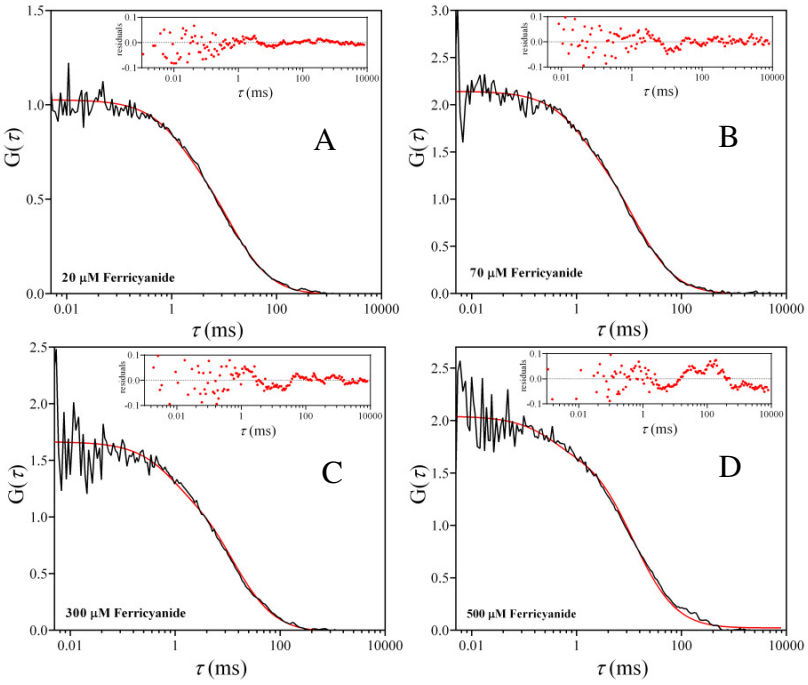

Figure 5.15: *Experimentally obtained ACFs of fraction 2 (K122S Cu azurin labeled with ATTO655) for samples containing 20 (A), 70 (B), 300 (C) and 500 (D) µM hexacyanoferrate (III). The red lines are fits according to Eqn. 3.4* $G(\tau) = G(0).G_{diff}(\tau).G_1(\tau)$ *with* $\tau_D = 12$ *ms.*

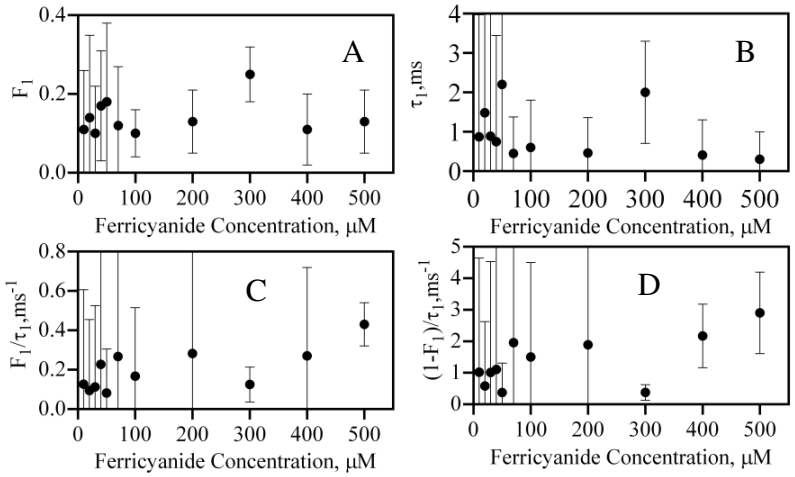

Figure 5.16: *(A) and (B): Parameters* (F_1 *and* τ_1) *obtained by fitting the ACFs of K122S labeled Cu azurin (fraction 2) as a function of the concentration of added hexacyanoferrate (III). The equation used for the fits was* $G(\tau) = G(0).G_{diff}(\tau).G_1(\tau)$ *with* $\tau_D = 12$ *ms. (C) and (D):* $F_1/\tau_1 = k^f$ *and* $(1-F_1)/\tau_1 = k^b$ *are plotted as a function of potassium hexacyanoferrate (III) concentrations, respectively. Vertical bars denote 95% confidence intervals.*

Applying the same formalism as discussed in Chapter 4 and for K122Q under scheme 5.1, one

obtains k_1^f = 8×10^4 s^{-1} and k_1^b = 1.5×10^3 s^{-1}. As before (See Chapter 4), these values can be used to obtain the reorganization energy for electron transfer. We obtained driving forces of ΔG_f = -0.476 eV and ΔG_b = -1.384 eV for the reactions shown in Scheme 5.1. This, finally leads (See details in Chapter 4) to λ (K122S) = 0.75 eV.

5.3.4.4 K122S Cu Azurin-ATTO655, fraction 2, under reducing conditions

The observations for K122S CuAzurin-ATTO655, fraction 2, were comparable to K122Q species 2. For each time trace the autocorrelation function was calculated. Application of $G(\tau) = G(0)\ G_{diff}(\tau)$ and/ or $G(\tau) = G(0)\ G_{diff}(\tau)\ G_1(\tau)$ produced fits with a noticeable non-random component (Fig. 5.17). Therefore, the ACFs were fit with an equation containing the additional term, $G_2(\tau)$, ($G(\tau) = G(0)\ G_{diff}(\tau)\ G_1(\tau)\ G_2(\tau)$) (Eqn. 5.1) with the diffusion correlation time fixed at τ_D = 12 ms (Fig. 5.18). The amplitudes F_1 and F_2, and the corresponding correlation times, τ_1 and τ_2, are presented in Fig. 5.19. The same scheme 5.2 can be applied here.

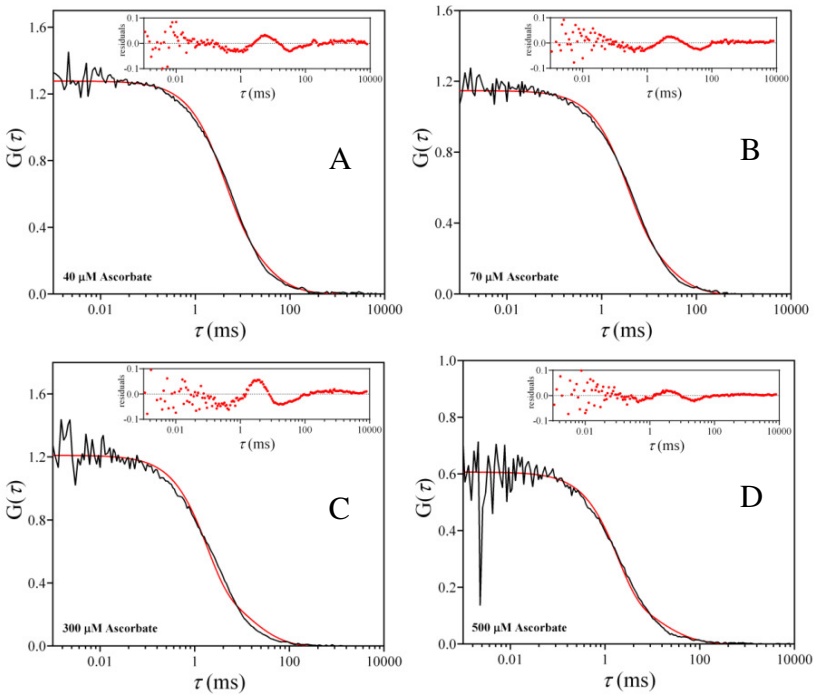

Figure 5.17: *Experimentally obtained ACFs of species 2 from K122S Cu azurin labeled with ATTO655 for samples containing 40 (A), 70 (B), 300 (C) and 500 (D) µM ascorbate. The red lines are fits according to Eqn. 3.4 $G(\tau) = G(0).G_{diff}(\tau).G_1(\tau)$ with τ_D =12 ms. The residuals of the fits in the insets show unsatisfactory fitting of the ACFs.*

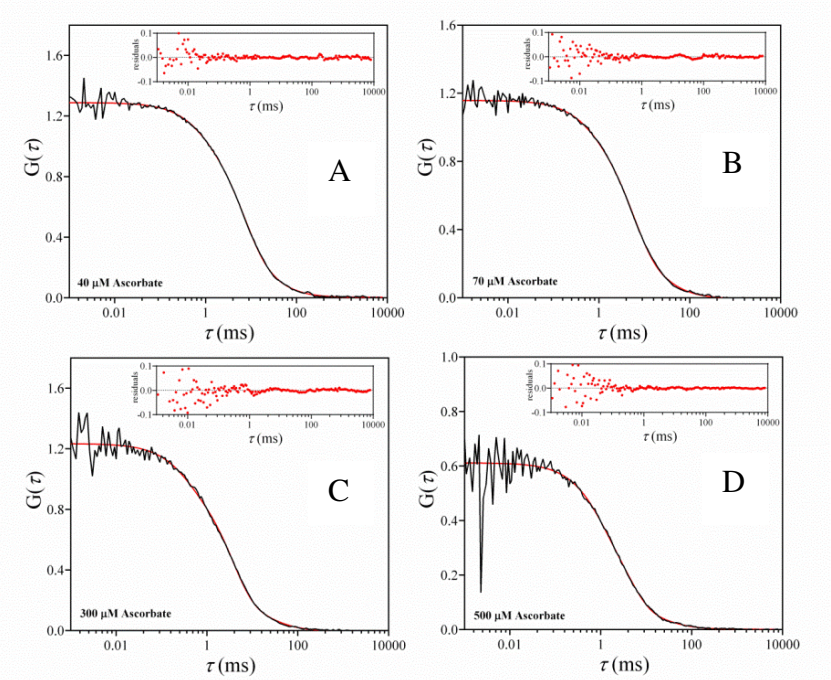

Figure 5.18: *Experimentally obtained ACFs of fraction 2 from K122S Cu azurin labeled with ATTO655 for samples containing 40 (A), 70 (B), 300 (C) and 500 (D) µM ascorbate. The red lines are fits according to Eqn. 5.1 $G(\tau) = G(0).G_{diff}(\tau).G_1(\tau)\ G_2(\tau)$ with τ_D =12 ms. The residuals of the fits (See insets) show satisfactory fitting of the ACFs.*

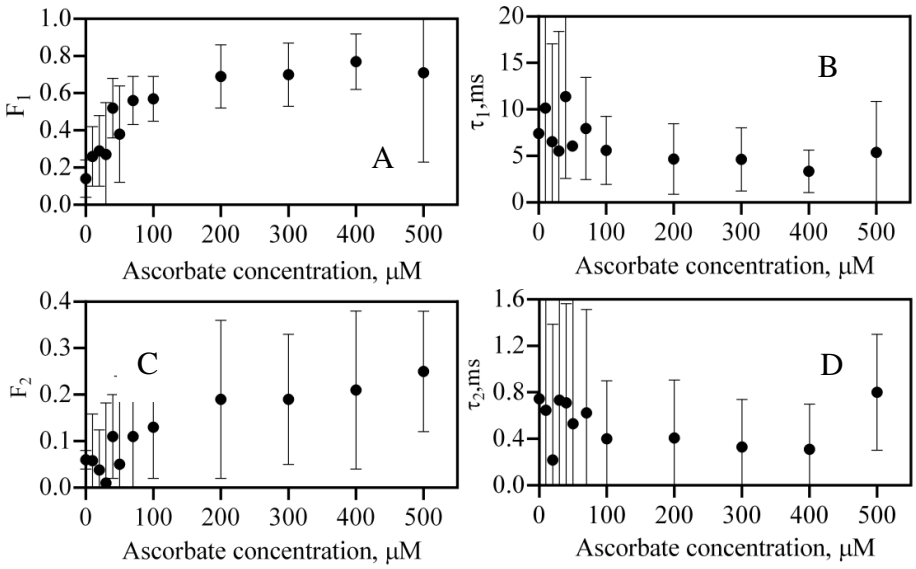

Figure 5.19: *Parameters obtained from the fits of the ACFs of K122S Cu azurin-ATTO655, fraction 2. The equation used was $G(\tau) = G_{diff}(\tau)\ G_1(\tau)\ G_2(\tau)$ with τ_D =12 ms. Shown are, as function of ascorbate concentration: F_1 (A), τ_1 (B), F_2 (C), and τ_2 (D).*

As discussed in Chapter 4, consistent with the intramolecular character of the reaction, τ_2 appears independent of the reductant concentration. The fraction of dark molecules F_2, increases with reductant concentration. The issue of dissolved oxygen in the solution has already been discussed in the previous chapter (see Chapter 4 for details). As seen from the analysis, F_2, as obtained from the fits, is not constant. Only with excess of ascorbate, F_2 approaches a constant value. Applying the same formalism (Chapter 4) to find k_2^f and k_2^b, we find,

$F_2/\tau_2 = f(I)\ k_2^f$ and

$(1-F_2)/\tau_2 = k_2^b$

Applying the same formalism for the K122S variant (see Chapter 4), we find $k_2^f = 1.1\times10^5$ s^{-1} and $k_2^b = 1.8\times10^3$ s^{-1} with $F_2 = 0.23$, $\tau_2 = 0.45$ ms. The resulting intramolecular ET rates are presented in Table 5.2.

	$L^*\rightarrow Cu(II)$	$Cu(I)\rightarrow L^+$	$Cu(I)\rightarrow L^*$	$L^-\rightarrow Cu(II)$
Sample	k_1^f, s^{-1} (a)	k_1^b, s^{-1} (a)	k_2^f, s^{-1} (b)	k_2^b, s^{-1} (b)
K122Q Cu-azurin	8.0×10^4	1.5×10^3	2.1×10^5	3.3×10^3
K122S Cu-azurin	6.1×10^4	1.2×10^3	1.1×10^5	1.8×10^3
wt Cu azurin[#] labeled at K122	4.8×10^4	0.7×10^3	3.3×10^6	1.0×10^4

(#) see Chapter 4, page 120, Table 4.1

Table 5.2: *Experimentally obtained intramolecular rate constants for K122Q and K122S-species 2 and K122 labeled wt Cu azurin.*

(a) in presence of excess of hexacyanoferrate (III) and

(b) in presence of excess of ascorbate

Using those experimentally obtained forward and backward rate constants and $E_{ATTO/ATTO^-}$ = -0.17 V (vs NHE), $n_{ATTO} = 0$ and $n_{Cu(I)}=1$ and the values used in chapter 4 for the other parameters, one obtains λ (K122S) = 1.05 eV under reducing conditions.

F_1 and τ_1 are analysed as before (Chapter 4 for details), taking into account that only a fraction

(1-F_2) of the labeled molecules is in the bright state. Based on the value of $f(I,)$ we can again estimate $k_r f(I)$. The data for $k_r f(I)$ and k_b have been gathered in Table 5.3.

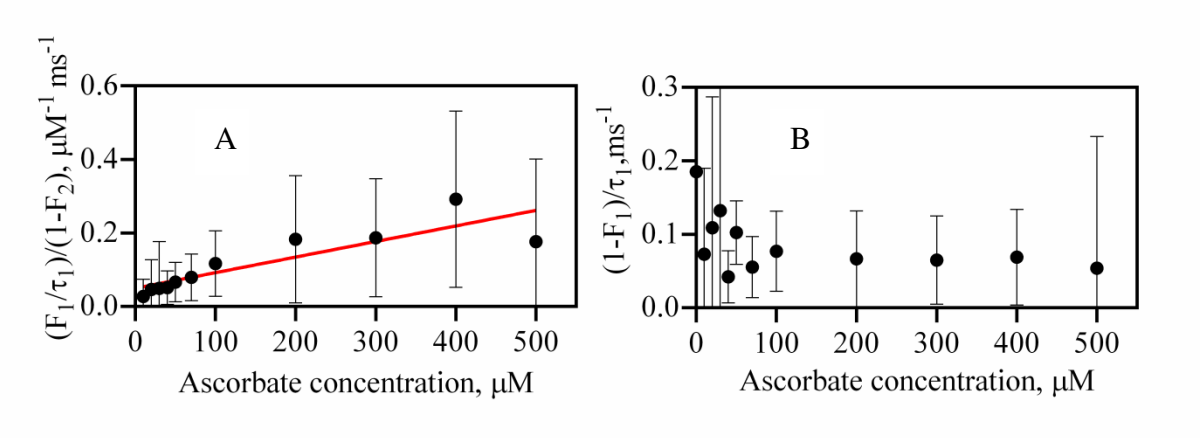

Figure 5.20: *Analysis of the ACFs of labeled Cu azurin variant (K122S). ACFs were fitted with the equation $G(\tau) = G(0)\, G_{diff}(\tau)\, G_1(\tau)\, G_2(\tau)$ with $\tau_D = 12$ ms. Parameters τ_1 and F_1, as obtained from the fits, correspond with $G_1(\tau)$. (A) $(F_1/\tau_1)/(1-F_2)$ $(=k_f)$ as a function of the concentration of ascorbate (B) $(1-F_1)/\tau_1$ $(=k_b)$ as a function of the concentration of ascorbate for the same variants. The red straight line in (A) is a least-squares fit to the data points.*

Species	$k_r f(I), M^{-1}s^{-1}$	k_b, s^{-1}
K122Q-species 2	$(3.4\pm0.7)\times10^5$	$(9.6\pm4.0)\times10^1$
K122S-species 2	$(4.2\pm0.8)\times10^5$	$(6.6\pm1.5)\times10^1$
wt Cu azurin labeled at K122[#]	$(2.0\pm0.3)\times10^5$	$(5.6\pm0.6)\times10^1$
wt Cu azurin labeled at N-terminus[#]	$(3.2\pm0.3)\times10^5$	$(3.5\pm0.2)\times10^1$

(#) see Chapter 4, page 120, Table 4.1

Table 5.3: *Experimental values of $k_r f(I)$ and k_b for CuAzurin (wt and the variants) in presence of reducing agents (ascorbate). See text and Chapter 4 for further explanations.*

Species	*Oxidizing condition(a)*	*Reducing condition(b)*
K122Q-species 2	0.76	1.08
K122S-species 2	0.75	1.05
Wt azurin labeled at K122[#]	0.75	1.16

(#) see Chapter 4 for details

Table 5.4*: Experimental values of reorganization energies (eV) for Cu Azurin (wt and the variants) in presence of redox agents (ascorbate). See text and Chapter 4 for further explanations.*

(a) in presence of potassium hexacyanoferrate (III)

(b) in presence of ascorbate

5.4 *Comparison of fluorescence resonance energy transfer (FRET) and photoinduced electron-transfer (PET) reaction in Copper Azurin-ATTO655*

In view of the increasing use of fluorescence labeling of biomolecules *in vivo* and *in vitro* the quenching of dye fluorescence in a labeled protein is an important subject. FRET and PET may occur simultaneously and it will be helpful to obtain an idea when PET may be expected to occur and when not. Whereas the FRET between ATTO655 and the Cu(II) center occurs on the nanosecond scale, the PET occurs on the microsecond-sub-millisecond scale, several orders of magnitude larger than FRET. With the experimental data (ΔG, λ for the wild type and the variants of azurin) in hand, we can calculate the dependence of the FRET and PET rates on the Cu-label distance in the azurin-ATTO655 system. Calculations of the two rates (k_{FRET} and k_{ET}) have been performed over a distance from 0 to 80 Å of the Cu-label system.

Calculation of the rate of FRET (k_{FRET}) was performed using the following equation:

$$k_{FRET} = \frac{1}{\tau_L}\left(\frac{R_0}{R}\right)^6 \qquad (5.3)$$

where τ_L is the lifetime of the fluorescent donor in the absence of the acceptor (ATTO655 in sucrose, 2.7 ns), R_0 is the Förster radius of the ATTO655-azurin pair and R is the donor-acceptor distance. The so-called Förster radius is given by (*43*)

$$R_0 = 0.211[\kappa^2 n^{-4} Q_D J(\lambda)]^{1/6} \qquad (5.4)$$

where R_0 is the distance at which the transfer efficiency is at 50% of its maximum value, Q_D is the fluorescence quantum yield of the donor in absence of the acceptor, n is the refractive index of the sample, κ is the orientation factor for the dipolar interaction and $J(\lambda)$ is the overlap integral which is given by (see Chapter 1, Eqn. 1.3)

$$J(\lambda) = \int_0^\infty I_D(\lambda)\varepsilon_A(\lambda)\lambda^4 d\lambda \,/\, \int_0^\infty I_D(\lambda)d\lambda$$

The spectral calculator in the Quick Fit 3.0 software was used to obtain the FRET radius between Oxidized copper azurin and ATTO655. A value of R_0 of 37 Å was calculated for the donor-acceptor pair ATTO655-oxidized Cu Azurin, based on the absorption spectrum of the oxidized form of *wt* Cu Azurin and on the emission spectrum of ATTO655 measured experimentally(*43*)(*44*)(*45*).

Photoinduced electron transfer may occur next to FRET. For the calculation of the PET rates, two models are at our disposal: "Pathway model" and "Organic glass model".

When structural information is available a pathway can be delineated along which ET may be effectuated. The most efficient pathway is usually the shortest one that can be constructed. It will contain mostly covalent bonds with an occasional through space jump or a step comprising a hydrogen bond. The formula to calculate the ET rate according to this "pathway model" has been discussed already in Chapter 4 and is reproduced here(*46*)(*47*)

$$k_{ET} = 3 \times 10^{13} e^{-\beta_0 \sigma_C \ell} e^{-\frac{(\Delta G_f + \lambda)^2}{4\lambda kT}} \tag{5.5}$$

where, β_0 is the electron transfer attenuation factor (0.7, or 1.4 Å^{-1}, *vide infra*), ℓ is the length of a C-C bond (1.4 Å) and σ_C is the number of equivalent C-C bonds in the path, ΔG is the driving force for the electron transfer reaction, λ is the reorganization energy of the electron donor-electron acceptor system, k is Boltzmann's constant, T is the temperature in Kelvin.

In case, no detailed structural information on donor-acceptor pair is available or when donor and acceptor are not covalently linked, the "organic glass" model of Moser and Dutton may be applied according to which the ET through a protein can be linked to tunneling of

electron through an organic glass. The formula to calculate the ET rate according to this model is(*48*)(*49*):

$$\log k_{ET} = 13 - 0.6(R - 3.6) - (\Delta G + \lambda)^2/4\lambda kT \qquad (5.6)$$

where, ΔG is the driving force for the electron transfer reaction, λ is the reorganization energy of the electron donor-electron acceptor system, k is Boltzmann's constant, T is the temperature in Kelvin and R is the distance between donor and acceptor molecule. The coefficient "0.6" reflects the quantized nuclear term as provided by extensive studies in the photosynthetic reaction-centers. This pathway model might apply when the dye forms an association complex and an electron jumps directly from the dye to the copper center and vice versa.

The variation of PET and FRET rates over a distance from 0 to 80 Å for ATTO655 labeled Cu azurin is depicted in Fig. 5.21 when oxidizing conditions apply. Under reducing conditions, FRET between ATTO655 and the reduced Cu site in azurin does not occur, and it is likely that PET is the main event occurring upon excitation of the label. We have used the parameters that correspond with the case of CuAz-K122-ATTO655. The PET rates were calculated by using the experimentally obtained ΔG_f (free energy change for the ET reaction from the label to the metal center), ΔG_b (free energy change for the ET reaction from the label to the metal center) and λ (reorganization energy of ET reaction in wt CuAzurin-ATTO655) (Chapter 4 for details). Three different values of β_0 were used for the calculation of PET. β_0 = 1.0 $Å^{-1}$ reflects the situation encountered for the label on Lys122, where a clear through bound pathway is identifiable, whereas β_0 = 1.4 $Å^{-1}$ is more suitable to model the situation where the label is on Ala1 and an electron most likely would have to travel to the copper center through a mixed pathway (through bond as well as through space hops) (Fig. 5.21).

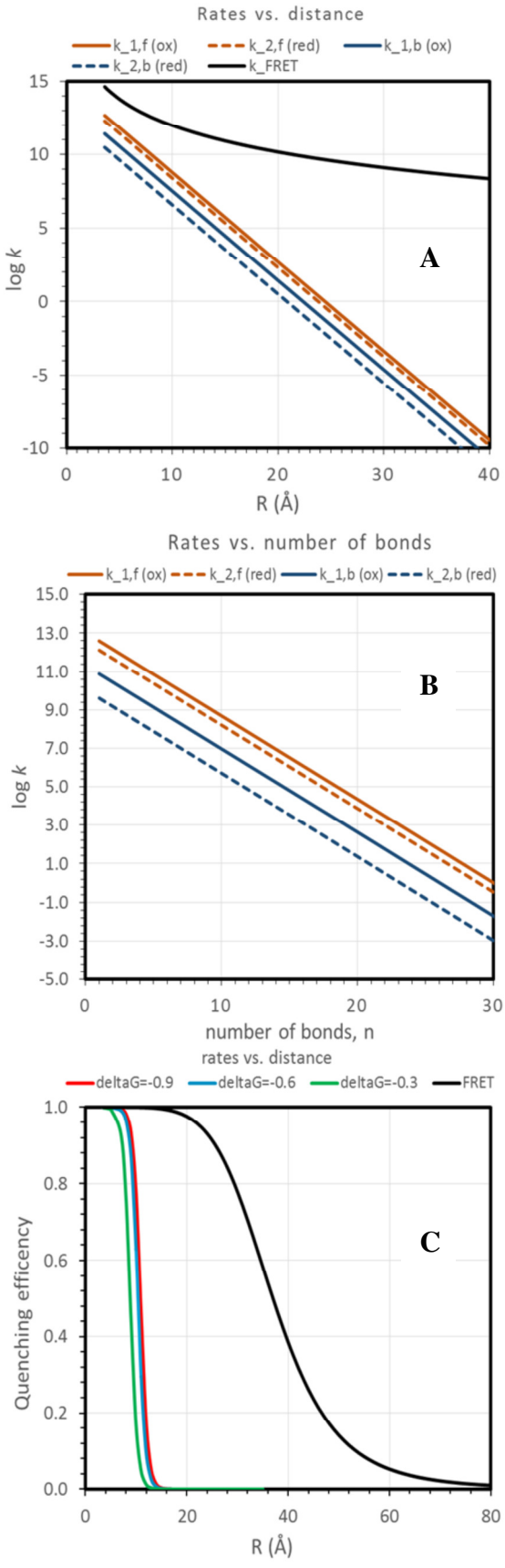

Figure 5.21: FRET and PET rates and quenching efficiencies for labeled azurin as a function of length parameters. (***A***). FRET (black) and PET quenching rates as a function of the distance R between Cu center and chromophore. The FRET rates were calculated with Eqn. 5.3 with a Förster radius R_0 = 37 Å and life time of the dye in the absence of quenching of τ = 2.7 ns. PET rates were calculated from $\log k_{ET} = 13 - 0.6(R - 3.6) - \frac{(\Delta G+\lambda)^2}{4\lambda kT}$ (*49*)with λ= 0.76 eV, and ΔG = −0.476 (k_1^f, red solid line); λ= 1.16 eV, and ΔG = −1.67 (k_2^f , red dashed line); λ= 0.76 eV, and ΔG = −1.384 (k_1^b, blue solid line); λ= 1.16 eV, and ΔG = –0.19 (k_2^b, blue dashed line)

(***B***). PET quenching rates as a function of the number of covalent bonds n between chromophore and Cu site. Rates were calculated from Eqn. 5.5(*50*)(*51*), with β_0 = 1 per bond. Different lines refer to similar cases as in panel (***A***). (***C***). Quenching efficiency $Q_E \equiv (F_0 - F)/F_0 = k/(k_0 + k)$ calculated as a function of distance between chromophore and Cu center. Here $k_0 = 1/\tau_L$ and k is either the PET or the FRET rate. FRET rates were calculated as in panel ***(A)***. PET rates were calculated as in panel ***(A)*** with λ = 0.90 eV and ΔG = −0.9, −0.6 and −0.3 eV (green, blue and red lines, respectively).

The data in panel **(C)** clearly show that quenching by PET is short ranged while FRET quenching extends over a much long range.

It is seen that PET may occur much more generally and may take place over large distances between the dye and the redox center in azurin. PET rates may slow down to 10^3 s^{-1} for pathways longer than 19±3 effective C-C bonds. In practice it means that when the label is more than 18 Å away from the copper and attached more than 17 equivalent bonds away from the copper center, PET quenching can be ignored for the type of experiments described in this thesis. The FRET rate, on the other hand, shows a much shallower distance dependence.

5.5 *Future prospects and concluding remarks*

In the present work a single-molecule based approach for the study of electron-transfer process within proteins was presented. In some of the isolated species an electron-transfer reaction between azurin and the attached ATTO655 is observed using FCS. In future, the position of the label in the variants will be established by mass spectrometry experiments. Improvements in the separation, as well as application of methods other than ion exchange chromatography will be useful for other proteins as well. A most important finding is the observation of ET reaction between the label and the metal center when the former is bound to surface lysines (Lys 24/Lys27/Lys128). Proximity of those lysines to the copper site makes it possible that either through-bond electron tunneling or back-folding of the label toward the surface of the protein allows transfer of electrons. As k_{ET} and λ have been determined experimentally and good estimates of ΔG are available, the electronic couplings between the donor and the acceptor can be extracted and its value can be compared with predictions from currently prevailing models.

Overall, we see that it be possible to encounter intramolecular ET reaction in Cu azurin-ATTO655 bioconjugates where the reaction sites can be surface lysines of azurin (Lys24, Lys27, Lys128, etc.) other than Lys122 and the time scale of intramolecular electron-transfer in those cases might not be similar to our previous results obtained in *wt* azurin. In case of the variants, no extra decay was observed in autocorrelation curves for the electron-transfer reactions and the inverse of k_{ET} is found in the sub-millisecond time scale. As the ET parameters (driving forces, reorganization energies) were determined experimentally for a number of cases (*wt* Cu azurin, K122S and K122Q), the variation of the rates with distance was calculated with ET-models and it was our additional interest to see how these rates compare to FRET promoted deactivation of

the excited labels. The PET rates observed in fraction 2 of K122S and K122Q Cu-Azurin indicate that the label is likely to be attached to the one of the lysine residues e.g. Lys 24/Lys27/Lys128 which is ≥ 20 Å away from the copper center. Previously, PET was thought to occur only when donor and acceptor are in Van-der-Waal contact. We show here that PET still may occur over large distances in labeled oxido-reductases. Thus, our study provides insights on discovery and characterization of long-range photo-induced electron-transfer processes in dye labeled proteins.

References

(1) Holm, R. H.; Kennepohl, P.; Solomon, E. I. Structural and Functional Aspects of Metal Sites in Biology. *Chem. Rev.* **1996**, *96*, 2239–2314.

(2) Thomson, A. J.; Gray, H. B. Bio-inorganic chemistry. *Curr. Opin. Chem. Biol.* **1998**, *2*, 155–158.

(3) Marcus, R. a.; Sutin, N. Electron transfers in chemistry and biology. *Biochim. Biophys. Acta - Rev. Bioenerg.* **1985**, *811*, 265–322.

(4) Kolczak, U., Dennison, C., Messerschmidt, A., and Canters, G. W. *Handbook of Metalloproteins*; 2001.

(5) Van de Kamp, M.; Hali, F. C.; Rosato, N.; Agro, A. F.; Canters, G. W. Purification and characterization of a non-reconstitutable azurin, obtained by heterologous expression of the Pseudomonas aeruginosa azu gene in Escherichia coli. *Biochim. Biophys. Acta* **1990**, *1019*, 283–292.

(6) Leckner, J.; Bonander, N.; Wittung-Stafshede, P.; Malmström, B. G.; Karlsson, B. G. The effect of the metal ion on the folding energetics of azurin: A comparison of the native, zinc and apoprotein. *Biochim. Biophys. Acta - Protein Struct. Mol. Enzymol.* **1997**, *1342*, 19–27.

(7) Carmelo Rosa, Danilo Milardi, Domenico Grasso, Rita Guzzi, L. S. Thermodynamics of the thermal unfolding of azurin. *J. Phys. Chem.* **1995**, *99*, 14864–14870.

(8) Engeseth, H. R.; McMillin, D. R. Studies of thermally induced denaturation of azurin and azurin derivatives by differential scanning calorimetry: evidence for copper selectivity. *Biochemistry* **1986**, *25*, 2448–2455.

(9) Palm-Espling, M. E.; Niemiec, M. S.; Wittung-Stafshede, P. Role of metal in folding and stability of copper proteins in vitro. *Biochim. Biophys. Acta - Mol. Cell Res.* **2012**, *1823*, 1594–1603.

(10) Kamp, M. Van De; Floris, R. Site-directed mutagenesis reveals that the hydrophobic patch of azurin mediates electron transfer. *J. Am. Chem. Soc.* **1990**, *112*, 907–908.

(11) Vijgenboom, E.; Busch, J. E.; Canters, G. W. In vivo studies disprove an obligatory role of azurin in denitrification in Pseudomonas aeruginosa and show that azu expression is under control of rpoS and ANR. *Microbiology* **1997**, *143 (Pt 9*, 2853–2863.

(12) Yamada, T.; Goto, M.; Punj, V.; Zaborina, O.; Kimbara, K.; Das Gupta, T. K.; Chakrabarty, a. M. The bacterial redox protein azurin induces apoptosis in J774 macrophages through complex formation and stabilization of the tumor suppressor protein p53. *Infect. Immun.* **2002**, *70*, 7054–7062.

(13) Tobin, P. H.; Wilson, C. J. Examining photoinduced energy transfer in pseudomonas aeruginosa azurin. *J. Am. Chem. Soc.* **2014**, *136*, 1793–1802.

(14) Farver, O.; Bonander, N.; Skov, L. K.; Pecht, I. The pH dependence of intramolecular electron transfer in azurins. *Inorganica Chim. Acta* **1996**, *243*, 127–133.

(15) Jensen, P. S.; Chi, Q.; Zhang, J.; Ulstrup, J. Long-Range interfacial electrochemical electron transfer of Pseudomonas aeruginosa azurin-gold nanoparticle hybrid systems. *J. Phys. Chem. C* **2009**, *113*, 13993–14000.

(16) Edman, L.; Mets, U.; Rigler, R. Conformational transitions monitored for single molecules in solution. *Proc. Natl. Acad. Sci. U. S. A.* **1996**, *93*, 6710–6715.

(17) Chen, P.; Andoy, N. M. Single-molecule fluorescence studies from a bioinorganic perspective. *Inorganica Chim. Acta* **2008**, *361*, 809–819.

(18) Wang, Q.; Goldsmith, R. H.; Jiang, Y.; Bockenhauer, S. D.; Moerner, W. E. Probing single biomolecules in solution using the anti-Brownian electrokinetic (ABEL) trap. *Acc. Chem. Res.* **2012**, *45*, 1955–64.

(19) Mollova, E. T. Single-molecule fluorescence of nucleic acids. *Curr. Opin. Chem. Biol.* **2002**, *6*, 823–828.

(20) Xie, X. S. Single-Molecule Approach to Enzymology. *Single Mol.* **2001**, *2*, 229–236.

(21) Haustein, E.; Schwille, P. Ultrasensitive investigations of biological systems by fluorescence correlation spectroscopy. *Methods* **2003**, *29*, 153–166.

(22) Chiantia, S.; Ries, J.; Schwille, P. Fluorescence correlation spectroscopy in membrane structure elucidation. *Biochim. Biophys. Acta* **2009**, *1788*, 225–233.

(23) Kapusta, P.; Macháň, R.; Benda, A.; Hof, M. Fluorescence lifetime correlation spectroscopy (FLCS): Concepts, applications and outlook. *Int. J. Mol. Sci.* **2012**, *13*, 12890–12910.

(24) Ries, J.; Schwille, P. Fluorescence correlation spectroscopy. *Bioessays* **2012**, *34*, 361–8.

(25) Elson, E. L. Fluorescence correlation spectroscopy: Past, present, future. *Biophys. J.* **2011**, *101*, 2855–2870.

(26) Krichevsky, O. Fluorescence correlation spectroscopy : the technique. *Rep.Prog.Phys* **2002**, *65*, 251.

(27) Hess, S. T.; Huang, S.; Heikal, A. A.; Webb, W. W. Biological and chemical applications of fluorescence correlation spectroscopy: A review. *Biochemistry* **2002**, *41*, 697–705.

(28) Magde, D.; Elson, E.; Webb, W. W. Thermodynamic fluctuations in a reacting system measurement by fluorescence correlation spectroscopy. *Phys. Rev. Lett.* **1972**, *29*, 705–708.

(29) Schmauder, R.; Librizzi, F.; Canters, G. W.; Schmidt, T.; Aartsma, T. J. The oxidation state of a protein observed molecule-by-molecule. *Chemphyschem* **2005**, *6*, 1381–6.

(30) Schmauder, R.; Alagaratnam, S.; Chan, C.; Schmidt, T.; Canters, G. W.; Aartsma, T. J. Sensitive detection of the redox state of copper proteins using fluorescence. *J. Biol. Inorg. Chem.* **2005**, *10*, 683–687.

(31) Kuznetsova, S.; Zauner, G.; Schmauder, R.; Mayboroda, O. A.; Deelder, A. M.; Aartsma, T. J.; Canters, G. W. A Förster-resonance-energy transfer-based method for fluorescence detection of the protein redox state. *Anal. Biochem.* **2006**, *350*, 52–60.

(32) Tabares, L.; Gupta, A.; Aartsma, T.; Canters, G. Tracking Electrons in Biological Macromolecules: From Ensemble to Single Molecule. *Molecules* **2014**, *19*, 11660–11678.

(33) Goldsmith, R. H.; Tabares, L. C.; Kostrz, D.; Dennison, C.; Aartsma, T. J.; Canters, G. W.; Moerner, W. E. Redox cycling and kinetic analysis of single molecules of solution-phase nitrite reductase. *Proc. Natl. Acad. Sci. U. S. A.* **2011**, *108*, 17269–74.

(34) Nicolardi, S.; Andreoni, A.; Tabares, L. C.; Van Der Burgt, Y. E. M.; Canters, G. W.; Deelder, A. M.; Hensbergen, P. J. Top-down FTICR MS for the identification of fluorescent labeling efficiency and specificity of the Cu-protein azurin. *Anal. Chem.* **2012**, *84*, 2512–20.

(35) Robert C. Weast, M. J. A. *CRC Handbook of Chemistry and Physics*; CRC Press, Inc, Boca Raton, Florida.

(36) Goldberg, M.; Pecht, I. Kinetics and equilibria of the electron transfer between azurin and the hexacyanoiron (II/III) couple. *Biochemistry* **1976**, *15*, 4197–4208.

(37) Nicolardi, S.; Andreoni, A.; Tabares, L. C.; van der Burgt, Y. E. M.; Canters, G. W.; Deelder, A. M.; Hensbergen, P. J. Top-down FTICR MS for the identification of fluorescent labeling efficiency and specificity of the Cu-protein azurin. *Anal. Chem.* **2012**, *84*, 2512–20.

(38) Gilani, A. G.; Moghadam, M.; Hosseini, S. E.; Zakerhamidi, M. S. A comparative study on the aggregate formation of two oxazine dyes in aqueous and aqueous urea solutions. *Spectrochim. Acta, Part A* **2011**, *83*, 100–105.

(39) Monari, S.; Battistuzzi, G.; Dennison, C.; Borsari, M.; Ranieri, A.; Siwek, M. J.; Sola, M. Factors Affecting the Electron Transfer Properties of an Immobilized Cupredoxin. *J. Phys. Chem. C* **2010**, *114*, 22322–22329.

(40) Doose, S.; Neuweiler, H.; Sauer, M. Fluorescence quenching by photoinduced electron transfer: a reporter for conformational dynamics of macromolecules. *Chemphyschem A Eur. J. Chem. Phys. Phys. Chem.* **2009**, *10*, 1389–1398.

(41) Van de Kamp M1, Canters GW, Andrew CR, Sanders-Loehr J, Bender CJ, P. J. Effect of lysine ionization on the structure and electrochemical behaviour of the Met44-->Lys mutant of the blue-copper protein azurin from Pseudomonas aeruginosa. *Eur. J. Biochem.*

1993, *218*, 229–238.

(42) Clair, C. S.; Ellis, W.; Gray, H. Spectroelectrochemistry of blue copper proteins: pH and temperature dependences of the reduction potentials of five azurins. *Inorganica Chim. Acta* **1992**, *191*, 149–155.

(43) Lakowicz, J. R. *Principles of Fluorescence Spectroscopy*; 2006.

(44) L. Stryer Fluorescence energy-transfer as a spectroscopic ruler. *Annu. Rev. Biochem.* **1978**, *47*, 819–846.

(45) Jan Wolfgang Krieger and Jörg Langowski QuickFit 3.0: A data evaluation application for biophysics. **2015**.

(46) Devault, D. Quantum mechanical tunnelling in biological systems. *Q. Rev. Biophys.* **1980**, *13*, 387–564.

(47) Marcus, R. A. Electron Transfer Reactions in Chemistry: Theory and Experiment. *Angew. Chemie Int. Ed. English* **1993**, *32*, 1111–1121.

(48) Moser, C. C.; Keske, J. M.; Warncke, K.; Farid, R. S.; Dutton, P. L. Nature of biological electron transfer. *Nature* **1992**, *355*, 796–802.

(49) Page, C. C.; Moser, C. C.; Chen, X.; Dutton, P. L. Natural engineering principles of electron tunnelling in biological oxidation-reduction. *Nature* **1999**, *402*, 47–52.

(50) Canters, G. W.; van de Kamp, M. Protein-mediated electron transfer. *Curr. Opin. Struct. Biol.* **1992**, *2*, 859–869.

(51) J N Onuchic, D N Beratan, J R Winkler, H. B. G. Pathway analysis of protein electron-transfer reactions. *Annu. Rev. Biophys. Biomol. Struct.* **1992**, *21*, 349–377.